How to cite: *Angew. Chem. Int. Ed.* **2023**, *62*, e202307750
doi.org/10.1002/anie.202307750

Polycyclic Hydrocarbons

Twisted Diindeno-Fused Dibenzo[*a*,*h*]anthracene Derivatives and their Dianions

Yanwei Gu, Herdya S. Torchon, Yikun Zhu, Zheng Wei, Dieter Schollmeyer, Manfred Wagner, Yong Ni, Zehua Wu, Hao Wu, Yazhou Zhou, Zijie Qiu, Marina A. Petrukhina,* and Klaus Müllen**

Abstract: We report a facile synthesis of diindeno-fused dibenzo[a,h]anthracene derivatives (**DIDBA-2Cl**, **DIDBA-2Ph**, and **DIDBA-2H)** with different degrees of non-planarity using three substituents (chloro, phenyl, and hydrogen) of various sizes. The planarization of their cores, as evidenced by the decreased end-to-end torsional angles, was confirmed by X-ray crystallography. Their enhanced energy gaps with twisting were investigated by a combination of spectroscopic and electrochemical methods with density functional theory, which showed a transition from singlet open-shell to closed-shell configuration. Moreover, their doubly reduced states, **DIDBA-2Ph**$^{2-}$ and **DIDBA-2H**$^{2-}$, were achieved by chemical reduction. The structures of dianions were identified by X-ray crystallographic analysis, which elucidated that the electron charging further distorted the backbones. The electronic structure of the dianions was demonstrated by experimental and theoretical approaches, suggesting decreased energy gaps with larger non-planarity, different from the neutral species.

Introduction

The rational design of diindeno-fused polycyclic hydrocarbons (PHs) allows for the fine-tuning of their electronic structures.[1] Their construction connecting two indeno units by different π-conjugated spacers has been reported to modulate the bonding situation.[2] For instance, in contrast to benzene and naphthalene,[3] larger bridges built from anthracene, phenanthrene, and bischrysene endow diindeno-fused PHs with open-shell singlet diradical character (Figure 1a).[4] Open-shell molecules exhibit a narrow energy gap, redox amphotericity, large two-photon absorption, and thermally activated paramagnetism, making them promising candidates for applications in organic electronics, nonlinear optics, spintronics, and energy storage devices.[5]

An interesting comparison can be made when looking at twisted [n]acenes which possess higher stability and solubility than the parent compounds (Figure 1b).[6] In addition, twisted π-conjugated chromophores showing smaller energy gaps of S_1–T_1 excited states can be applied in thermally activated delayed fluorescent materials.[7] To tailor the electronic structure of diindeno-fused PHs by twisting the skeleton, we selected the diindeno-fused dibenzo-[*a*,*h*]anthracene (**DIDBA**, Figure 1c). Spin-unrestricted density functional theory (DFT) calculations (UB3LYP/6-31G-(d,p)) predict that the parent **DIDBA** has an open-shell singlet ground state with a diradical character index (y_0) of 0.25 (see Supporting Information (SI), Table S1) owing to the recovery of aromaticity at the central benzene ring and the spin-polarization at the terminal carbon atoms (Figure S3a in SI).[1b]

[*] Prof. Dr. Y. Gu, Dr. M. Wagner, Dr. Z. Wu, Dr. H. Wu, Prof. Dr. Y. Zhou, Prof. Dr. Z. Qiu, Prof. Dr. K. Müllen
Synthetic Chemistry, Max Planck Institute for Polymer Research
Ackermannweg 10, 55128 Mainz (Germany)
E-mail: muellen@mpip-mainz.mpg.de

H. S. Torchon, Y. Zhu, Dr. Z. Wei, Prof. Dr. M. A. Petrukhina
Department of Chemistry, University at Albany, State University of New York
1400 Washington Ave, Albany, NY 12222 (USA)
E-mail: mpetrukhina@albany.edu

Prof. Dr. Y. Gu
Ningbo Institute of Materials Technology & Engineering, Chinese Academy of Sciences
Ningbo, Zhejiang, 315201 (P. R. China)
E-mail: guyanwei@nimte.ac.cn

Prof. Dr. K. Müllen
Institute for Physical Chemistry, Johannes Gutenberg University Mainz
Duesbergweg 10–14, 55128 Mainz (Germany)

Dr. D. Schollmeyer
Department of chemistry, Johannes Gutenberg University Mainz
Duesbergweg 10–14, 55128 Mainz (Germany)

Prof. Dr. Y. Ni
Department of Chemistry, Southern University of Science and Technology
Shenzhen, Guangdong, 518055 (P. R. China)

© 2023 The Authors. Angewandte Chemie International Edition published by Wiley-VCH GmbH. This is an open access article under the terms of the Creative Commons Attribution License, which permits use, distribution and reproduction in any medium, provided the original work is properly cited.

© 2023 The Authors. Angewandte Chemie International Edition published by Wiley-VCH GmbH

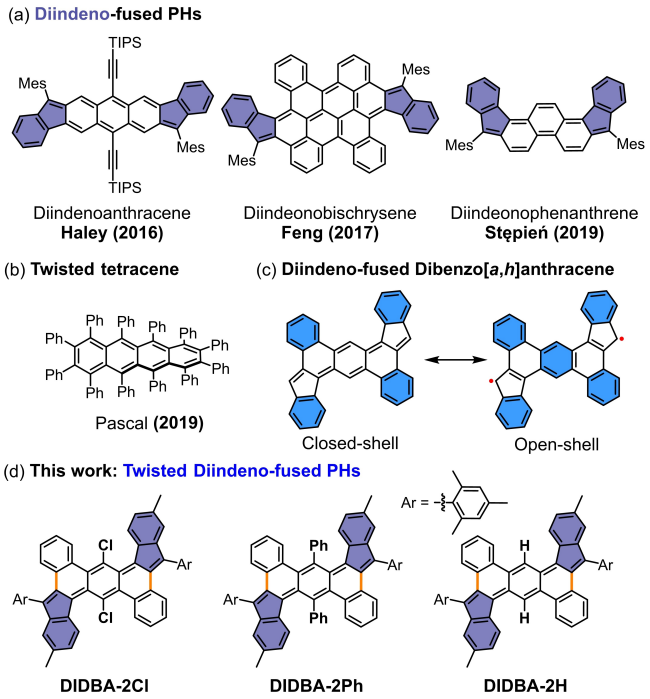

Figure 1. (a) Examples of diindeno-fused PHs with various π-conjugated spacers. (b) Twisted tetracene. (c) Resonance structure of diindeno-fused dibenzo[*a*,*h*]anthracene (**DIDBA**). (d) Structures of twisted **DIDBA-2Cl**, **DIDBA-2Ph**, and **DIDBA-2H** with various sizes of substituents at the peripheral positions of the central benzene ring.

Herein, the title compounds **DIDBA-2Cl**, **DIDBA-2Ph**, and **DIDBA-2H** (Figure 1d) were generated by introducing different substituents (chloro, phenyl, and hydrogen) of different sizes at the peripheral positions of the central benzene ring. The degree of twisting was quantitively evaluated from the torsional angles between a set of bonds (labeled with orange color) at both ends of the anthracene. The electronic structure, geometry, and aromaticity of three compounds were elucidated by a combination of experimental and theoretical approaches including X-ray crystallography, ^{1}H NMR spectroscopy, electron-spin resonance (ESR) spectrometry, UV/Vis-NIR absorption, and cyclic voltammetry. Additionally, doubly reduced **DIDBA-2Ph**$^{2-}$ and **DIDBA-2H**$^{2-}$ were achieved through alkali metal reduction, revealing the effect of electron charging on their backbones and aromaticity. The impact of twisting on the electronic structure of charged species was also investigated.

Results and Discussion

The synthesis started with the Suzuki coupling between **1a**–**b** (1,4-dibromo-2,5-dichlorobenzene and 2′,5′-dibromo-’, 1′:4″1″-terphenyl) and (2-(*p*-tolylethynyl)phenyl)boronic acid (**2**) to afford compounds **3a**–**b**, as described in Scheme 1. Followed by cyclization with iodine monochloride, the benzotetraphene backbones with chloro/phenyl substituents **4a**–**b** were achieved at −78 °C in quantitative yield. The treatment of **4a**–**b** with *n*-butyllithium and subsequently mesitaldehyde furnished diol intermediates,

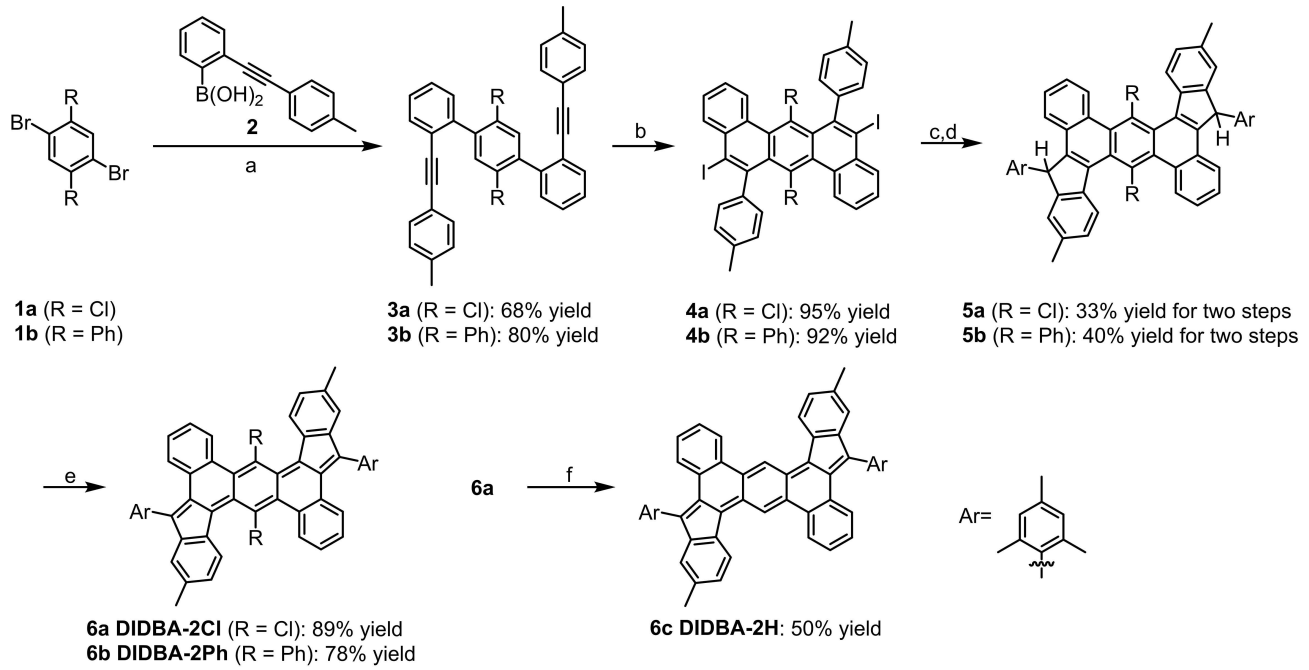

Scheme 1. Synthetic route toward **DIDBA-2Cl**, **DIDBA-2Ph**, and **DIDBA-2H**. Reagents and Conditions: (a) tetrakis(triphenylphosphine)palladium(0), potassium carbonate, dioxane/water, 80 °C/36 h for **1a**, 90 °C/12 h for **1b**; (b) iodine monochloride, dichloromethane, −78 °C, 1 h; (c) i) *n*-butyllithium, tetrahydrofuran, −78 °C, 1.5 h; ii) mesitaldehyde, rt, 12 h; (d) boron trifluoride diethyl etherate, dichloromethane, 0 °C to rt, 1 h; (e) i) potassium *tert*-butoxide, dimethylformamide, 10 min; ii) *p*-chloranil, 2 h; (f) allyl[1,3-bis(2,6-diisopropylphenyl)imidazol-2-ylidene]chloropalladium(II), sodium *tert*-butoxide, tetrahydrofuran, isopropyl alcohol, 60 °C, 1 h.

© 2023 The Authors. Angewandte Chemie International Edition published by Wiley-VCH GmbH

15213773, 2023, 34, Downloaded from https://onlinelibrary.wiley.com/doi/10.1002/anie.202307750 by MPI 355 Polymer Research, Wiley Online Library on [22/08/2023]. See the Terms and Conditions (https://onlinelibrary.wiley.com/terms-and-conditions) on Wiley Online Library for rules of use; OA articles are governed by the applicable Creative Commons License

which could be directly used in the next Friedel–Crafts cyclization catalyzed by boron trifluoride diethyl etherate to generate dihydro precursors **5a–b**. Finally, dehydrogenation with a mixture of potassium *tert*-butoxide and dimethylformamide in situ yielded a radical anion, which was further oxidized with *p*-chloranil to obtain the desired products **DIDBA-2Cl** (**6a**) and **DIDBA-2Ph** (**6b**) as dark purple solids. To obtain the target molecule **DIDBA-2H** (**6c**), a similar synthetic method (1,4-bromobenzene as starting material) was adopted. However, the iodine monochloride-induced cyclization generated two isomers confirmed by high-performance liquid chromatography (Figure S1 in SI). Although a similar backbone of **DIDBA-2H** was reported with another synthetic method,[8] one facile strategy to obtain **DIDBA-2H** here started directly from **DIDBA-2Cl** with palladium catalyzed-hydrodechlorination. Different conditions for hydrodechlorination were reported,[9] but only the catalyst allyl[1,3-bis(2,6-diisopropylphenyl)imidazol-2-ylidene]chloropalladium(II) was feasible in this case.[10]

Single crystals suitable for X-ray crystallographic analysis were obtained by slow gas phase diffusion of methanol into the chloroform/dichloromethane solution of **DIDBA-2Cl/DIDBA-2Ph**, respectively. Unfortunately, the crystals of **DIDBA-2H** were of inferior quality, rendering them barely suitable for structure proof. As a result, its bond lengths had to be determined theoretically. The chloro substituents dramatically distort the skeleton compared with the phenyl group proton cases, as deduced from the larger end-to-end torsional angle (77.5°) of bonds *e*/*e'* (Figure 2a). Due to the highly twisted backbone without a symmetry plane and inversion center, **DIDBA-2Cl** possesses two mirror-image configurations (Figure 2b). Similarly, **DIDBA-2Ph** also displays R_a/S_a-configurations in the unit cell with a ratio of 1:1 (Figure 2b), consistent with the dynamic interconversion process for R_a/S_a-enantiomers in solution detected by NMR spectroscopies technique (see below). **DIDBA-2H** shows a planar backbone with only one configuration in the unit cell. Compared with two highly twisted derivatives, the longer *g*/*l* bonds and smaller bond length alternation of the extended *p*-quinodimethane unit (Figure 2c) in **DIDBA-2H** indicate

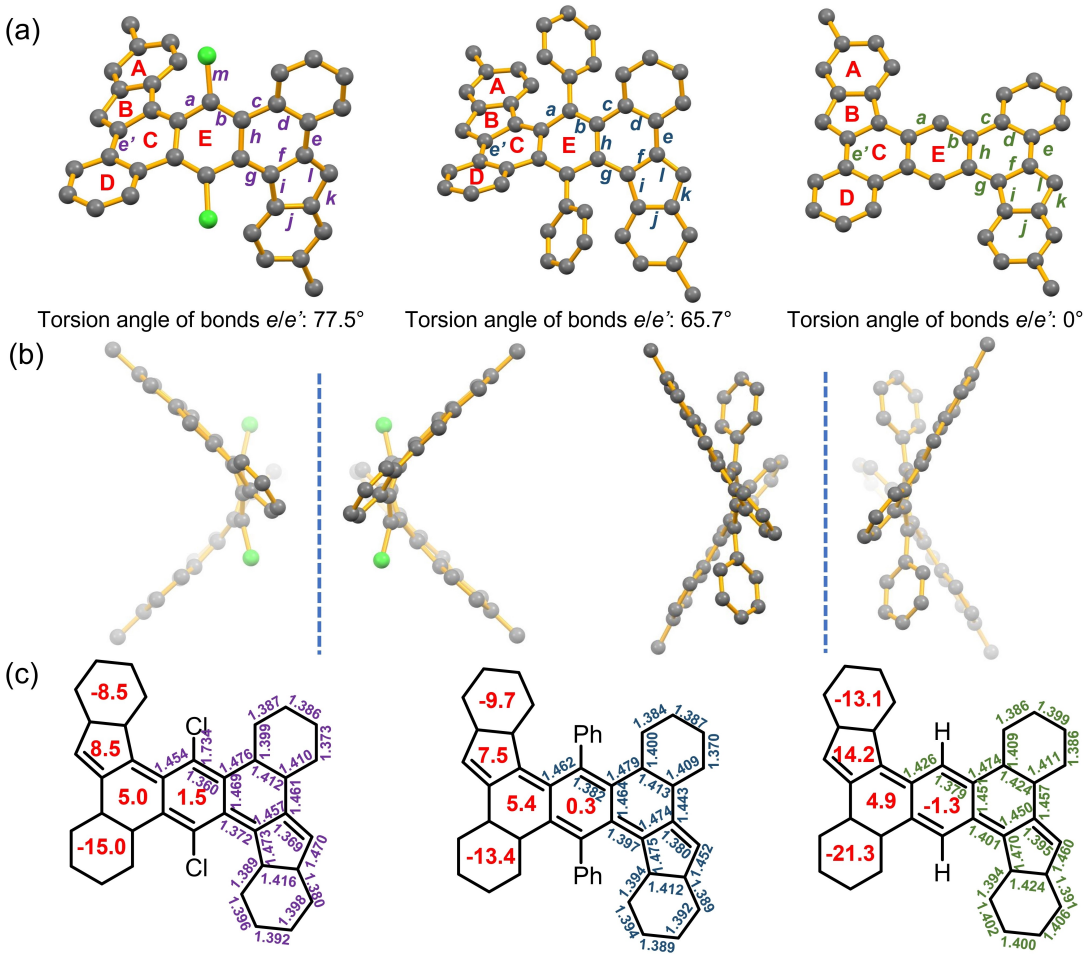

Figure 2. (a) The front view of **DIDBA-2Cl**, **DIDBA-2Ph**, and **DIDBA-2H**; ball-and-stick models. Hydrogen atoms and mesityl groups are omitted for clarity.[11] (b) Two enantiomers of **DIDBA-2Cl** and **DIDBA-2Ph** in the solid state; ball-and-stick models. Hydrogen atoms and mesityl groups are omitted for clarity. (c) Selected bond lengths (in Å) in the π-conjugated skeleton are labeled, and the red numbers in the individual rings are the calculated $NICS(1)_{zz}$ values.

© 2023 The Authors. Angewandte Chemie International Edition published by Wiley-VCH GmbH

15213773, 2023, 34, Downloaded from https://onlinelibrary.wiley.com/doi/10.1002/anie.202307750 by MPI 355 Polymer Research, Wiley Online Library on [22/08/2023]. See the Terms and Conditions (https://onlinelibrary.wiley.com/terms-and-conditions) on Wiley Online Library for rules of use; OA articles are governed by the applicable Creative Commons License

the larger diradical character of the planar skeleton and aromatic character of the ring E. This is consistent with theoretical indices of singlet diradical character (Table S1 in SI)[12] and Nucleus-Independent Chemical Shift[13] values ($NICS(1)_{zz}$, Figure 2c). The larger positive $NICS(1)_{zz}$ value of rings B/C indicates the antiaromatic character of the three structures.

In the solid state, **DIDBA-2Cl** displays a one-dimensional halogen-bonding chain with a distance of 3.26 Å between two chloro substituents, shorter than the sum (3.5 Å) of their van der Waals radii (Figure 3a). The halogen bond is derived from a significant σ-hole character of atoms interacting with an electron donor.[14] To study the electrostatic potential (ESP)[15] of **DIDBA-2Cl**, the structure was optimized at the B3LYP/6-31G(d,p) level, and the result was visualized with Multiwfn[16] and VMD[17] programs. In Figure 3b, **DIDBA-2Cl** exhibits a σ-hole with a relatively positive charge (δ^+, red) at the end of chloro substituents and a negative charge (δ^-, blue) on the surrounding of σ-hole.[18] The attraction between positive and negative charges leads to the one-dimensional chain. The intermolecular interaction was characterized by the isosurface of IGMH (independent gradient model based on Hirshfeld partition) analysis,[19] revealing that the major intermolecular interaction regions correspond to the weak attractive interactions between two chloro substituents (green area, Figure 3c).

DIDBA-2H showed a well-resolved ^{1}H NMR spectrum at 298 K in 1,2-dichlorobenzene-d_4 (Figure S62 in SI). The temperature dependence of ^{1}H NMR signals is an experimental indicator of singlet diradical character because a thermally excited triplet species leads to the broadening of signals. However, an appreciable peak broadening of **DIDBA-2H** was not observed when heating the solution to 433 K due to the small diradical character and large thermal population $\Delta E_{S\text{-}T}$ gap in this temperature range. The magnetic property of **DIDBA-2H** was further investigated by variable-temperature (VT) ESR measurement (Figure 4a). It displayed an unresolved one-line ESR spectrum with g_e of 2.00267, implying carbon-centered π-radicals. The signal intensity gradually increased upon raising the temperature, consistent with its open-shell singlet ground state. Fitting of the VT ESR data recorded in the solid by the Bleaney–Bowers equation[20] gave a singlet-triplet gap ($\Delta E_{S\text{-}T}$) of -8.16 ± 0.65 kcal/mol (Figure 4b). Calculations (UCAM-B3LYP/6-31G(d,p)) of the singlet diradical demonstrate that the spins are well distributed along the diindeno-fused anthracene unit (Figure S3b in SI). Compounds **DIDBA-2Cl** and **DIDBA-2Ph** failed to display ESR signals due to their closed-shell ground states. Thus, the effect of twisting plays a critical role in determining the electronic structure and magnetic properties of the title systems.

VT NMR spectra of compound **DIDBA-2Ph** were recorded in 1,1,2,2-tetrachloroethane-d_2. Notably, the NMR spectrum still exhibited a well-resolved signal in 413 K, while two peaks were gradually broadened and merged, indicating a dynamic interconversion process (Figure 5a). At 358 K, two split doublets were observed in a relative intensity of 1:1, which can be assigned to a pair of protons 4 and 8 based on two-dimensional NMR nuclear Overhauser effect spectroscopy (NOESY) (Figures S58–59 in SI), indicating that

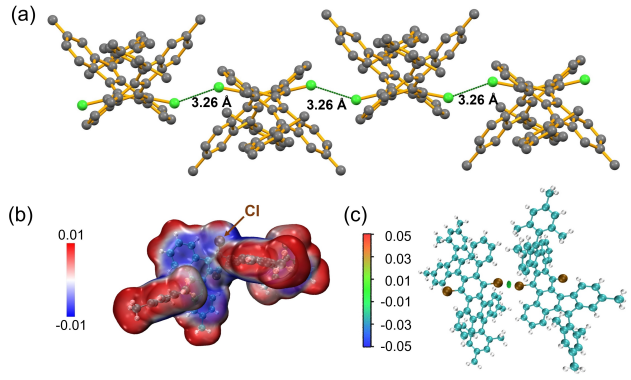

Figure 3. (a) One-dimensional halogen-halogen-bonding chain in the crystal. (b) Electrostatic potential (ESP) map of **DIDBA-2Cl**, blue and red represent electron-rich (negative value) and electron-deficient (positive value) regions, respectively. (c) Intermolecular interaction analysis for **DIDBA-2Cl**, and the corresponding isosurface by IGMH, where blue, green, and red represent strong attractive interactions, weak attractive interactions, and repulsive interactions.

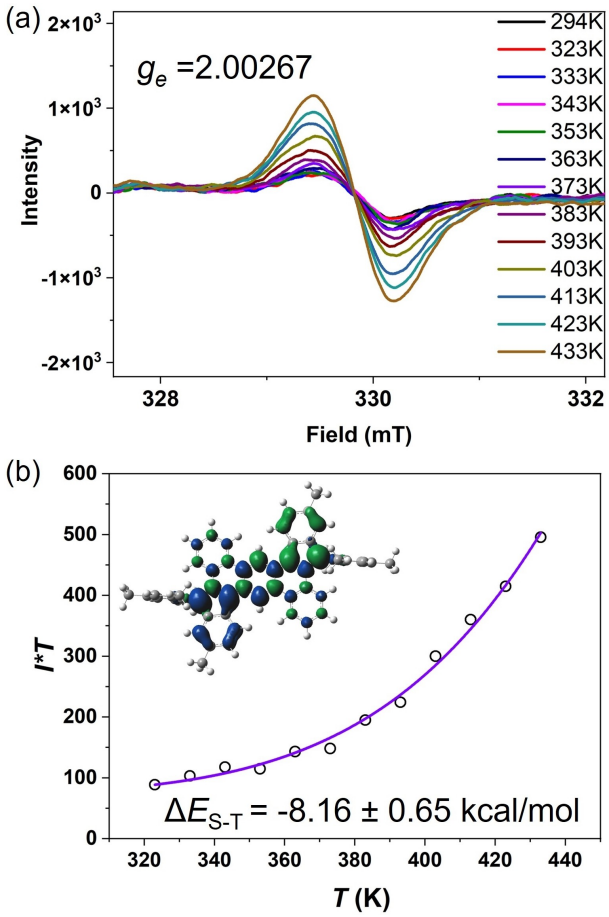

Figure 4. (a) VT ESR spectra and (b) *IT*–*T* plot of a solid sample of **DIDBA-2H**. *I*: integrated ESR intensity; and *T*: temperature in K. The violet line in (b) is the fitted curve, and the inset is the calculated spin-density distribution map of the singlet diradical.

© 2023 The Authors. Angewandte Chemie International Edition published by Wiley-VCH GmbH

15213773, 2023, 34, Downloaded from https://onlinelibrary.wiley.com/doi/10.1002/anie.202307750 by MPI 355 Polymer Research, Wiley Online Library on [22/08/2023]. See the Terms and Conditions (https://onlinelibrary.wiley.com/terms-and-conditions) on Wiley Online Library for rules of use; OA articles are governed by the applicable Creative Commons License

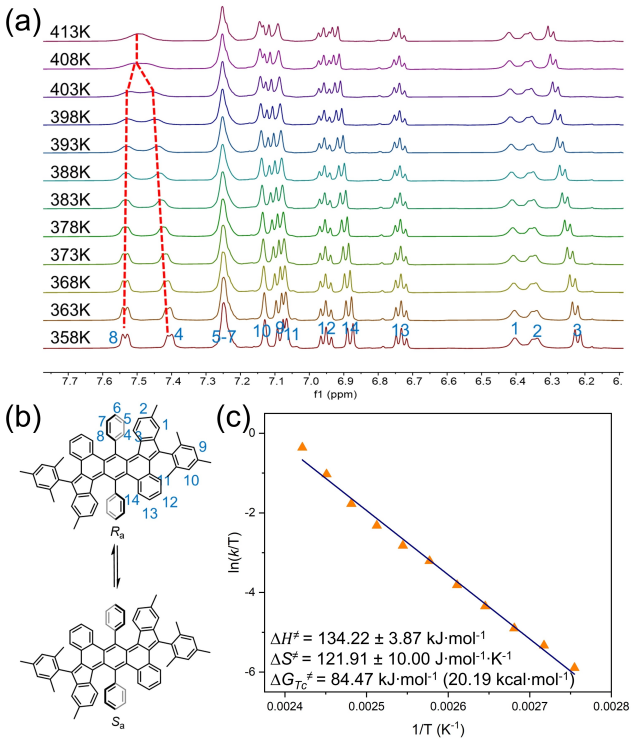

Figure 5. (a) VT ^{1}H NMR spectra (aromatic region) of **DIDBA-2Ph** in 1,1,2,2-tetrachloroethane-d_2. (b) The exchange between the R_a and S_a enantiomers. (c) Kinetic analysis of the exchange rate constants at different temperatures using the Eyring equation.

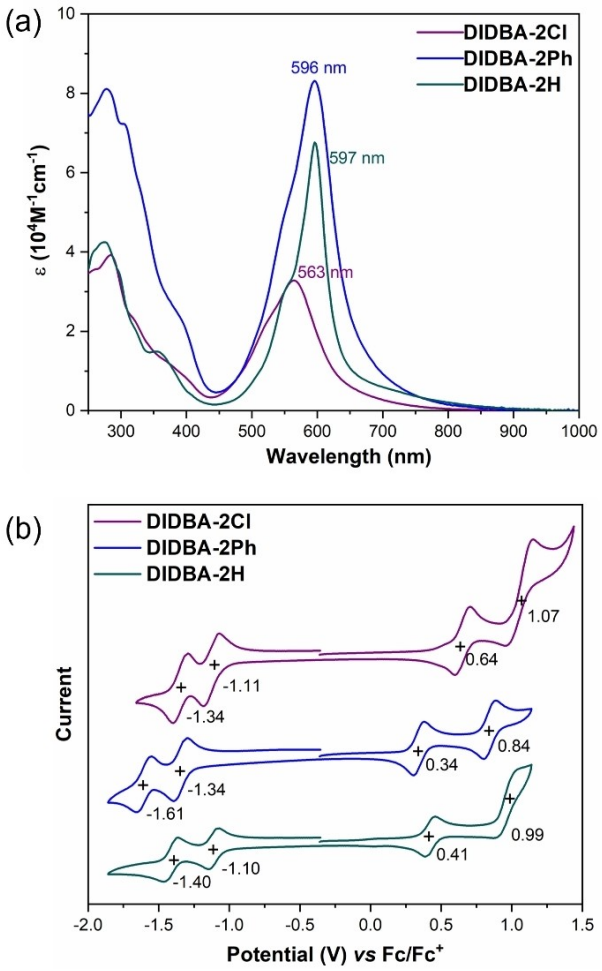

Figure 6. (a) UV/Vis-NIR absorption spectra of **DIDBA-2Cl**, **DIDBA-2Ph**, and **DIDBA-2H** in dichloromethane ($c = 2\times10^{-5}$ M). (b) Cyclic voltammograms of **DIDBA-2Cl**, **DIDBA-2Ph**, and **DIDBA-2H** in dichloromethane.

the rotation of phenyl rings of **DIDBA-2Ph** is slow on an NMR timescale (Figure 5b). Upon raising the temperature, two doublets (4 and 8) tended to merge together and coalesced at around 408 K. Further heating of the solution led to a well-resolved spectrum with only one set of sharp peaks due to the exchange between R_a-/S_a-isomers being rapid on the NMR timescale. The R_a-/S_a-exchange rate constants (k [s^{-1}]) in the temperature range from 358 to 413 K were then estimated by line-shape analysis of a pair of protons 4 and 8 (Table S9 in SI).[21] The interconversion rate constants k were plotted versus the reciprocal absolute temperature ($1/T$), and the data were then fitted by the Eyring equation $\ln\frac{k}{T} = -\frac{\Delta H^{\neq}}{RT} + \frac{\Delta S^{\neq}}{R} + \ln\frac{k_B}{h}$ to give the thermodynamic activation parameters $\Delta H^{\neq} = 134.22 \pm 3.87$ kJ·mol^{-1} and $\Delta S^{\neq} = 121.91 \pm 10.00$ J·mol^{-1}·K^{-1} (Figure 5c). The rotational energy barrier at the coalescence temperature $\Delta G_{Tc}^{\neq}$ ($T_c = 408$ K) was then estimated to be 84.47 kJ·mol^{-1} (20.19 kcal·mol^{-1}).

The UV/Vis-NIR absorption spectra of three compounds in dichloromethane (DCM) are shown in Figure 6a. **DIDBA-2Cl**, **DIDBA-2Ph**, and **DIDBA-2H** display similar higher-energy transitions in the 250–300 nm range with the maximum-wavelength absorption bands at 563, 596, and 597 nm, respectively. Calculations by time-dependent density functional theory (TD-DFT) (B3LYP/6-31G(d,p)) indicate that this maximum-wavelength absorption band originates from the HOMO-2→LUMO and HOMO→LUMO electronic transitions (Table S2–4 in SI). Moreover, the weak long tails extending to 800–900 nm of three compounds are attributed to the forbidden HOMO-1→LUMO electronic transition, which results from the inherent antiaromatic character of diindeno-fused PHs[1d,3c] rather than from the open-shell character which is only seen in **DIDBA-2H**. The cyclic voltammogram of **DIDBA-2Cl**, **DIDBA-2Ph**, and **DIDBA-2H** (Figure 6b) all exhibited two redox waves, from which the electrochemical energy gaps are estimated to be 1. 75 eV, 1. 68 eV, and 1.51 eV for **DIDBA-2Cl**, **DIDBA-2Ph**, and **DIDBA-2H**, respectively, which are consistent with the calculated HOMO–LUMO energy gaps (Figure S2 in SI). This implies that twisting the geometry leads to enhanced energy gaps in this diindeno-fused system with antiaromaticity.

The reversible reductive wave for three compounds observed electrochemically implies that the doubly reduced products could be accessed under the alkali metal reduction. Due to the presence of potentially reactive chloro substituents under the reaction conditions used, only compounds **DIDBA-2Ph** and **DIDBA-2H** were utilized for further

© 2023 The Authors. Angewandte Chemie International Edition published by Wiley-VCH GmbH

15213773, 2023, 34, Downloaded from https://onlinelibrary.wiley.com/doi/10.1002/anie.202307750 by MPI 355 Polymer Research, Wiley Online Library on [22/08/2023]. See the Terms and Conditions (https://onlinelibrary.wiley.com/terms-and-conditions) on Wiley Online Library for rules of use; OA articles are governed by the applicable Creative Commons License

chemical reduction. Their dianions were readily synthesized with excess sodium metal in anhydrous THF in the presence of [2.2.2]cryptand and 18-crown-6 ether, respectively, at room temperature (Scheme 2). The single crystals were obtained in moderate yield by slow diffusion of hexanes into THF solutions at 5 °C (See the Supporting Information for details).

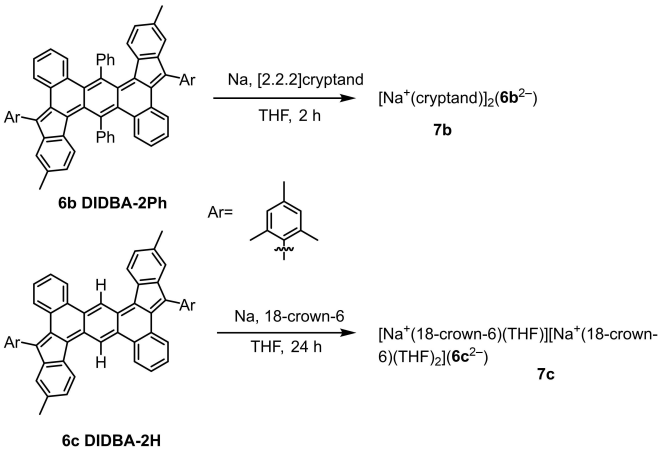

Scheme 2. Chemical reduction of **DIDBA-2Ph** and **DIDBA-2H** with sodium to afford the reduced products **7b** and **7c**.

The single crystal diffraction analysis (see more details in the SI) revealed the formation of a solvent-separated ion product (SSIP) of the doubly reduced anion with two Na^+-ions, namely {[Na^+(2.2.2-cryptand)]$_2$(**6b**$^{2-}$)} (**7b**), crystallized with three interstitial THF molecules as **7b**·3 C_4H_8O. Two cationic [Na^+(2.2.2-cryptand)] moieties are separated from the anionic core, providing a "naked" **DIDBA-2Ph**$^{2-}$ dianion (Figure 7a). Each Na^+ ion is wrapped by one [2.2.2]cryptand with the Na···O_{crypt} (2.438(4)–2.656(7) Å) and Na···N_{crypt} (2.601(4)–2.948(4) Å) distances comparable to the previously reported values.[22]

The crystal structure of **7c** (Figure 7b) consists of the doubly reduced anion and two Na^+-ions, {[Na^+(18-crown-6)(THF)][Na^+(18-crown-6)(THF)$_2$](**6c**$^{2-}$)}, crystallized with three interstitial THF molecules as **7c**·3 C_4H_8O. Two slightly different cationic moieties, [Na^+(18-crown-6)(THF)] and [Na^+(18-crown-6)(THF)$_2$], avoid the direct metal-π interactions, providing a "naked" **DIDBA-2H**$^{2-}$ anion. The

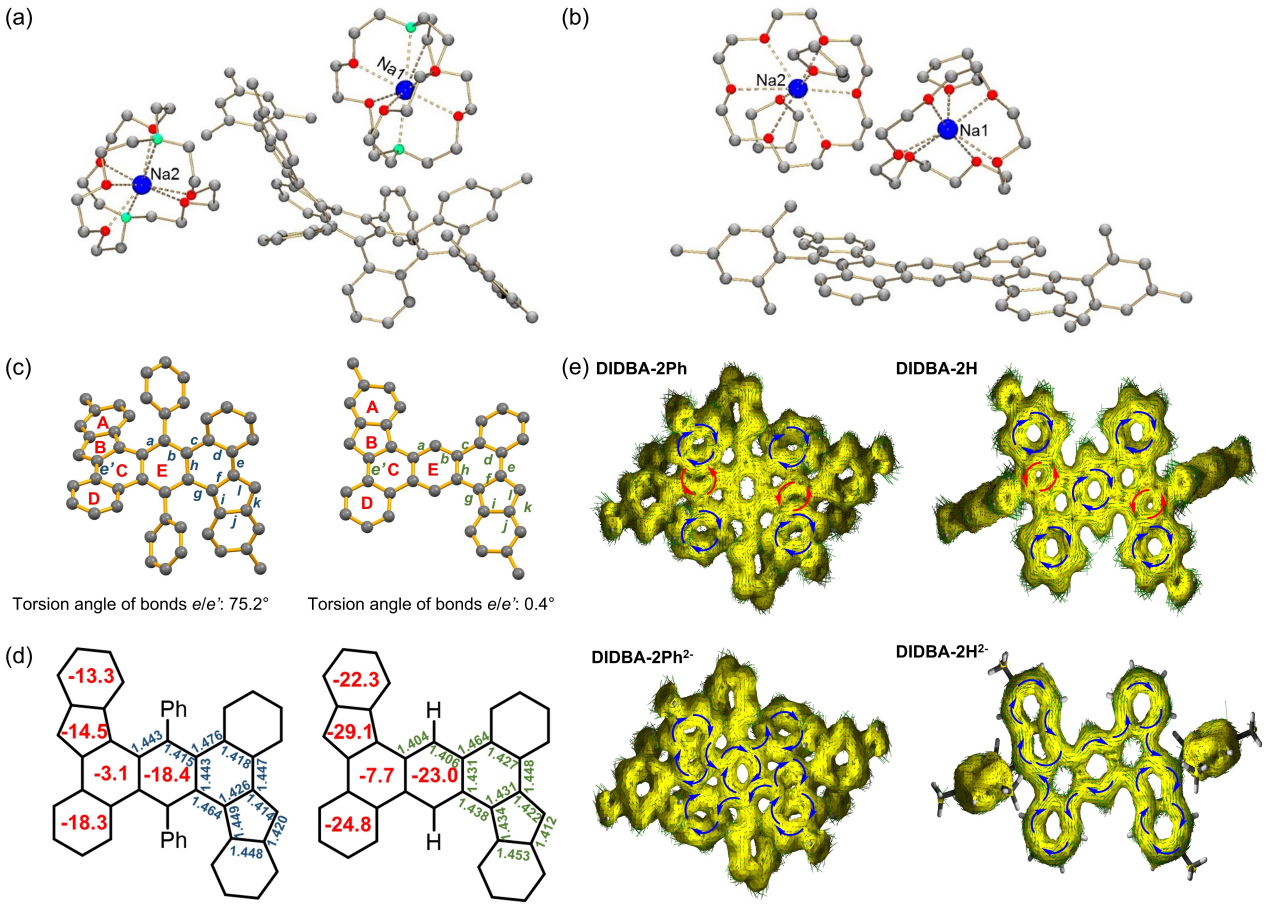

Figure 7. Crystal structures of (a) **7b** and (b) **7c**. Hydrogen atoms are omitted for clarity. Color scheme used: C gray, O red, Na blue, N spring green.[24] (c) The front view of **DIDBA-2Ph**$^{2-}$ and **DIDBA-2H**$^{2-}$; ball-and-stick model. Hydrogen atoms and mesityl groups are omitted for clarity. (d) Selected bond lengths (in Å) in the π-conjugated skeleton are labeled, and the red numbers in individual rings are the calculated NICS(1)$_{zz}$ values. (e) Calculated ACID plot (isovalue = 0.02, contribution from π electrons only) of neutral **DIDBA-2Ph** and **DIDBA-2H** and their dianion congeners **DIDBA-2Ph**$^{2-}$ and **DIDBA-2H**$^{2-}$.

© 2023 The Authors. Angewandte Chemie International Edition published by Wiley-VCH GmbH

15213773, 2023, 34, Downloaded from https://onlinelibrary.wiley.com/doi/10.1002/anie.202307750 by MPI 355 Polymer Research, Wiley Online Library on [22/08/2023]. See the Terms and Conditions (https://onlinelibrary.wiley.com/terms-and-conditions) on Wiley Online Library for rules of use; OA articles are governed by the applicable Creative Commons License

Na^+ ions are axially coordinated by one 18-crown-6 ether molecule and capped by one/two THF molecules with all $Na\cdots O_{crown}$ (2.429(8)–3.016(12) Å) and $Na\cdots O_{THF}$ (2.276(5)–2.385(7) Å) distances being similar to those previously reported.[23]

The electron charging dramatically distorts the skeleton of **DIDBA-2Ph**$^{2-}$, which is reflected by the increased end-to-end torsional angles of bonds *e*/*e'* (Figure 7c) due to two factors. On the one hand, the Coulomb repulsion among the delocalized negative charges of phenyl substituents and indeno units, presented by the calculated ESP maps (Figure S13 in SI), provides the driving force for the distortion. On the other hand, although no direct Na^+ ion binding is observed, multiple C–H···π interactions between the neighboring cations and the dianion contribute to the twisting of **DIDBA-2Ph**$^{2-}$ (Figures S21–22 in SI). Similarly, the multiple C–H···π interactions (Figures S23–24 in SI) slightly twisted the geometry of **DIDBA-2H**$^{2-}$ with the end-to-end torsion angle of 0.4°. Due to the twisted core with unsymmetrical torsional angles (Table S7 in SI), equimolar amounts of enantiomers were observed for **DIDBA-2Ph**$^{2-}$ and **DIDBA-2H**$^{2-}$ in the solid state (Figures S27–28 in SI).

Comparison of the C–C bonds of dianions with those of the neutral parent compounds demonstrates that the major changes are associated with the central part of the dicyclopenta[*a,h*]anthracene core. Particularly, the bonds *b*/*g*/*l*/*j* are elongated in both **DIDBA-2Ph**$^{2-}$ and **DIDBA-2H**$^{2-}$, while the adjacent bonds *a*/*h*/*f*/*i*/*k* become shortened. These structural changes lead to smaller bond length alternations implying enhanced aromaticity, which is theoretically confirmed by the negative $NICS(1)_{zz}$ values of rings B/C/E (Figure 7d). The Anisotropy of the Induced Current Density (ACID)[25] analyses of both dianions also reveal the change of aromaticity upon dianion formation (Figure 7e). For the **DIDBA-2Ph**$^{2-}$ and **DIDBA-2H**$^{2-}$, ACID plots show obvious diatropic ring currents (blue clockwise vector) along the periphery with partially localized current flows, thus indicating the global aromaticity. The enhanced aromaticity of the dianions is also experimentally reflected by the down-field chemical shift of protons in the aromatic regions of the ^1H NMR spectrum after the charging (see more details in the SI).

The UV/Vis spectra of the doubly reduced products display absorption peaks with λ_{max} at 586 nm in **DIDBA-2Ph**$^{2-}$ and 532 nm in **DIDBA-2H**$^{2-}$ (Figures S18 and S20 in SI). Compared with **DIDBA-2H**$^{2-}$, the bathochromic shifts of the maximum absorption in **DIDBA-2Ph**$^{2-}$ implies its smaller optical energy gap, in agreement with calculated HOMO–LUMO energy gaps of **DIDBA-2Ph**$^{2-}$ (2.06 eV) lower than that of **DIDBA-2H**$^{2-}$ (2.42 eV, Figure 8a). There are small variations for their HOMO energies, but the LUMO energies decrease upon twisting, consistent with previous reports that distortion of π-conjugation results in a substantial decrease of the LUMO energy for curved aromatics.[26] However, for the neutral compounds **DIDBA-2Ph** and **DIDBA-2H**, twisting the geometry significantly enhances the LUMO energy level (Figure 8b). The induced larger HOMO–LUMO energy gap reveals the opposite effect of twisting on the electronic structure of this diindeno-fused system in neutral and negatively charged states.

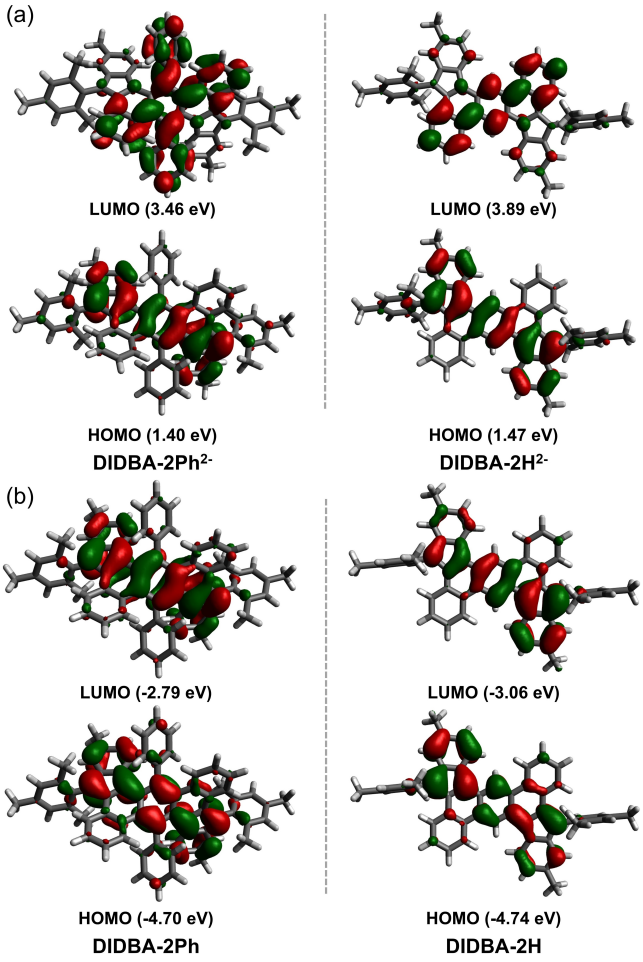

Figure 8. Calculated frontier molecular orbital profiles (isovalue = 0.02) of (a) charged **DIDBA-2Ph**$^{2-}$ and **DIDBA-2H**$^{2-}$ and (b) neutral **DIDBA-2Ph** and **DIDBA-2H**.

Conclusion

In summary, we have developed an efficient synthetic method to systematically bend the pristine diindeno-fused-polycyclic hydrocarbon **DIDBA** out of planarity by varying the size of the substituents at the peripheral position of the central benzene ring. X-ray crystallographic analysis of **DIDBA-2Cl**, **DIDBA-2Ph**, and **DIDBA-2H** reveals that the distorted backbone imposes chirality on the pristine structure, which is indeed seen from the existence of enantiomers in the solid state. Upon twisting, their enhanced energy gaps and decreased diradical character suggest a profound modulation of the bonding situation prevailing in diindeno-fused PHs. Furthermore, the chemical reduction furnishes the corresponding dianions **DIDBA-2Ph**$^{2-}$ and **DIDBA-2H**$^{2-}$ with global aromaticity. Remarkably therefore, their structural distortions are larger than those of the corre-

© 2023 The Authors. Angewandte Chemie International Edition published by Wiley-VCH GmbH

15213773, 2023, 34, Downloaded from https://onlinelibrary.wiley.com/doi/10.1002/anie.202307750 by MPI 355 Polymer Research, Wiley Online Library on [22/08/2023]. See the Terms and Conditions (https://onlinelibrary.wiley.com/terms-and-conditions) on Wiley Online Library for rules of use; OA articles are governed by the applicable Creative Commons License

sponding neutral species with antiaromaticity, and they display decreased energy gaps with larger non-planarity.

Different from reported methods to obtain non-planar diindeno-fused structures,[4b,c] our investigation offers novel access to extended π-conjugated frameworks with a high degree of twisting. The peripheral position of the central benzene ring in **DIDBA** provides the opportunity for the incorporation of additional units such as heterocycles,[27] an approach which is currently under investigation in our laboratory. As a result of their intrinsic chirality, redox potentials, as well as electronic and magnetic properties, these molecules can hold promise for chiral-induced spin selectivity,[28] energy storage, field-effect transistors,[29] and spintronics.

Acknowledgements

We are grateful to the financial support from the Max Planck Society, ERC grants on NANOGRAPH and 2DMATER, EU Projects GENIUS, and the EC under Graphene Flagship (No. CNECT-ICT-604391). Y. Gu acknowledges support from the Alexander von Humboldt Foundation. K.M. acknowledges a fellowship from Gutenberg Research College, Johannes Gutenberg University Mainz. Financial support of this work from the U. S. National Science Foundation, CHE-2003411, is gratefully acknowledged by M. A. P. NSF's ChemMatCARS, Sector 15 at the Advanced Photon Source (APS), Argonne National Laboratory (ANL) is supported by the Divisions of Chemistry (CHE) and Materials Research (DMR), National Science Foundation, under grant number NSF/CHE-1834750. Use of APS, an Office of Science User Facility operated for the U.S. Department of Energy (DOE) Office of Science by ANL, was supported by the U.S. DOE under Contract No. DE-AC02-06CH11357. Open Access funding enabled and organized by Projekt DEAL.

Conflict of Interest

The authors declare no conflict of interest.

Data Availability Statement

The data that support the findings of this study are available from the corresponding author upon reasonable request.

Keywords: Aromaticity · Dianions · Diradicals · Fused-Ring Systems · Twisted Structures

[1] a) M. Abe, *Chem. Rev.* **2013**, *113*, 7011–7088; b) Z. Zeng, X. Shi, C. Chi, J. T. Lopez Navarrete, J. Casado, J. Wu, *Chem. Soc. Rev.* **2015**, *44*, 6578–6596; c) H. Miyoshi, S. Nobusue, A. Shimizu, Y. Tobe, *Chem. Soc. Rev.* **2015**, *44*, 6560–6577; d) C. K. Frederickson, B. D. Rose, M. M. Haley, *Acc. Chem. Res.* **2017**, *50*, 977–987; e) X. Hu, W. Wang, D. Wang, Y. Zheng, *J. Mater. Chem. C* **2018**, *6*, 11232–11242; f) J. J. Dressler, M. M. Haley, *J. Phys. Org. Chem.* **2020**, *33*, e4114; g) J. Guo, X. Tian, Y. Wang, C. Dou, *Chem. Res. Chin. Univ.* **2023**, *39*, 161–169.

[2] a) X. Shi, P. M. Burrezo, S. Lee, W. Zhang, B. Zheng, G. Dai, J. Chang, J. T. López Navarrete, K.-W. Huang, D. Kim, J. Casado, C. Chi, *Chem. Sci.* **2014**, *5*, 4490–4503; b) K. Sbargoud, M. Mamada, J. Marrot, S. Tokito, A. Yassar, M. Frigoli, *Chem. Sci.* **2015**, *6*, 3402–3409; c) D. Hibi, K. Kitabayashi, K. Fujita, T. Takeda, Y. Tobe, *J. Org. Chem.* **2016**, *81*, 3735–3743; d) H. Miyoshi, M. Miki, S. Hirano, A. Shimizu, R. Kishi, K. Fukuda, D. Shiomi, K. Sato, T. Takui, I. Hisaki, M. Nakano, Y. Tobe, *J. Org. Chem.* **2017**, *82*, 1380–1388; e) J. J. Dressler, M. Teraoka, G. L. Espejo, R. Kishi, S. Takamuku, C. J. Gomez-Garcia, L. N. Zakharov, M. Nakano, J. Casado, M. M. Haley, *Nat. Chem.* **2018**, *10*, 1134–1140; f) P.-Y. Chen, Y.-C. Liu, H.-Y. Hung, M.-L. Pan, Y.-C. Wei, T.-C. Kuo, M.-J. Cheng, P.-T. Chou, M.-H. Chiang, Y.-T. Wu, *Org. Lett.* **2021**, *23*, 8794–8798; g) X. Xu, S. Takebayashi, H. Hanayama, S. Vasylevskyi, T. Onishi, T. Ohto, H. Tada, A. Narita, *J. Am. Chem. Soc.* **2023**, *145*, 3891–3896.

[3] a) D. T. Chase, A. G. Fix, B. D. Rose, C. D. Weber, S. Nobusue, C. E. Stockwell, L. N. Zakharov, M. C. Lonergan, M. M. Haley, *Angew. Chem. Int. Ed.* **2011**, *50*, 11103–11106; b) D. T. Chase, B. D. Rose, S. P. McClintock, L. N. Zakharov, M. M. Haley, *Angew. Chem. Int. Ed.* **2011**, *50*, 1127–1130; c) J. E. Barker, C. K. Frederickson, M. H. Jones, L. N. Zakharov, M. M. Haley, *Org. Lett.* **2017**, *19*, 5312–5315.

[4] a) G. E. Rudebusch, J. L. Zafra, K. Jorner, K. Fukuda, J. L. Marshall, I. Arrechea-Marcos, G. L. Espejo, R. Ponce Ortiz, C. J. Gomez-Garcia, L. N. Zakharov, M. Nakano, H. Ottosson, J. Casado, M. M. Haley, *Nat. Chem.* **2016**, *8*, 753–759; b) J. Ma, J. Liu, M. Baumgarten, Y. Fu, Y. Z. Tan, K. S. Schellhammer, F. Ortmann, G. Cuniberti, H. Komber, R. Berger, K. Mullen, X. Feng, *Angew. Chem. Int. Ed.* **2017**, *56*, 3280–3284; c) Y. C. Hsieh, C. F. Wu, Y. T. Chen, C. T. Fang, C. S. Wang, C. H. Li, L. Y. Chen, M. J. Cheng, C. C. Chueh, P. T. Chou, Y. T. Wu, *J. Am. Chem. Soc.* **2018**, *140*, 14357–14366; d) M. A. Majewski, P. J. Chmielewski, A. Chien, Y. Hong, T. Lis, M. Witwicki, D. Kim, P. M. Zimmerman, M. Stepien, *Chem. Sci.* **2019**, *10*, 3413–3420; e) R. Q. Lu, S. Wu, L. L. Yang, W. B. Gao, H. Qu, X. Y. Wang, J. B. Chen, C. Tang, H. Y. Shi, X. Y. Cao, *Angew. Chem. Int. Ed.* **2019**, *58*, 7600–7605.

[5] a) K. Kato, A. Osuka, *Angew. Chem. Int. Ed.* **2019**, *58*, 8978–8986; b) F. Lombardi, A. Lodi, J. Ma, J. Liu, M. Slota, A. Narita, W. K. Myers, K. Müllen, X. Feng, L. Bogani, *Science* **2019**, *366*, 1107–1110; c) Z. X. Chen, Y. Li, F. Huang, *Chem* **2021**, *7*, 288–332; d) W. Zeng, J. Wu, *Chem* **2021**, *7*, 358–386.

[6] a) J. E. Norton, K. N. Houk, *J. Am. Chem. Soc.* **2005**, *127*, 4162–4163; b) R. A. Pascal, *Chem. Rev.* **2006**, *106*, 4809–4819; c) J. Xiao, Y. Divayana, Q. Zhang, H. M. Doung, H. Zhang, F. Boey, X. W. Sun, F. Wudl, *J. Mater. Chem.* **2010**, *20*, 8167–8170; d) F. G. Brunetti, J. L. López, C. Atienza, N. Martín, *J. Mater. Chem.* **2012**, *22*, 4188–4205.

[7] X.-K. Chen, D. Kim, J.-L. Brédas, *Acc. Chem. Res.* **2018**, *51*, 2215–2224.

[8] S. S. K. Boominathan, K. H. Chang, Y. C. Liu, C. S. Wang, C. F. Wu, M. H. Chiang, P. T. Chou, Y. T. Wu, *Chem. Eur. J.* **2019**, *25*, 7280–7284.

[9] a) Y. Yamamoto, H. Matsubara, H. Yorimitsu, A. Osuka, *ChemCatChem* **2016**, *8*, 2317–2320; b) N. Fukui, S. K. Lee, K. Kato, D. Shimizu, T. Tanaka, S. Lee, H. Yorimitsu, D. Kim, A. Osuka, *Chem. Sci.* **2016**, *7*, 4059–4066.

[10] O. Navarro, H. Kaur, P. Mahjoor, S. P. Nolan, *J. Org. Chem.* **2004**, *69*, 3173–3180.

[11] Deposition numbers 2239353, 2239354, and 2239355 (for **DIDBA-2H**, **DIDBA-2Cl**, and **DIDBA-2Ph**) contain the

© 2023 The Authors. Angewandte Chemie International Edition published by Wiley-VCH GmbH

15213773, 2023, 34, Downloaded from https://onlinelibrary.wiley.com/doi/10.1002/anie.202307750 by MPI 355 Polymer Research, Wiley Online Library on [22/08/2023]. See the Terms and Conditions (https://onlinelibrary.wiley.com/terms-and-conditions) on Wiley Online Library for rules of use; OA articles are governed by the applicable Creative Commons License

supplementary crystallographic data for this paper. These data are provided free of charge by the joint Cambridge Crystallographic Data Centre and Fachinformationszentrum Karlsruhe Access Structures service.

[12] a) M. Nakano, R. Kishi, T. Nitta, T. Kubo, K. Nakasuji, K. Kamada, K. Ohta, B. Champagne, E. Botek, K. Yamaguchi, *J. Phys. Chem. A* **2005**, *109*, 885–891; b) M. Nakano, H. Fukui, T. Minami, K. Yoneda, Y. Shigeta, R. Kishi, B. Champagne, E. Botek, T. Kubo, K. Ohta, K. Kamada, *Theor. Chem. Acc.* **2011**, *130*, 711–724; c) T. Minami, M. Nakano, *J. Phys. Chem. Lett.* **2012**, *3*, 145–150.

[13] Z. Chen, C. S. Wannere, C. Corminboeuf, R. Puchta, P. v. R. Schleyer, *Chem. Rev.* **2005**, *105*, 3842–3888.

[14] P. Politzer, J. S. Murray, M. C. Concha, *J. Mol. Model.* **2008**, *14*, 659–665.

[15] J. Zhang, T. Lu, *Phys. Chem. Chem. Phys.* **2021**, *23*, 20323–20328.

[16] T. Lu, F. Chen, *J. Comput. Chem.* **2012**, *33*, 580–592.

[17] W. Humphrey, A. Dalke, K. Schulten, *J. Mol. Graphics* **1996**, *14*, 33–38.

[18] a) P. Metrangolo, F. Meyer, T. Pilati, G. Resnati, G. Terraneo, *Angew. Chem. Int. Ed.* **2008**, *47*, 6114–6127; b) G. Cavallo, P. Metrangolo, T. Pilati, G. Resnati, M. Sansotera, G. Terraneo, *Chem. Soc. Rev.* **2010**, *39*, 3772–3783; c) L. C. Gilday, S. W. Robinson, T. A. Barendt, M. J. Langton, B. R. Mullaney, P. D. Beer, *Chem. Rev.* **2015**, *115*, 7118–7195; d) M. H. Kolar, P. Hobza, *Chem. Rev.* **2016**, *116*, 5155–5187; e) J. Y. C. Lim, P. D. Beer, *Chem* **2018**, *4*, 731–783.

[19] T. Lu, Q. Chen, *J. Comput. Chem.* **2022**, *43*, 539–555.

[20] B. Bleaney, K. D. Bowers, *Proc. R. Soc. London Ser. A* **1952**, *214*, 451–465.

[21] F. P. Gasparro, N. H. Kolodny, *J. Chem. Educ.* **1977**, *54*, 258.

[22] a) N. K. Dalley, J. S. Bradshaw, X. Kou, R. M. Izatt, K. E. Krakowiak, *J. Heterocycl. Chem.* **1995**, *32*, 1201–1204; b) D. V. Konarev, M. A. Faraonov, A. V. Kuzmin, S. S. Khasanov, Y. Nakano, S. I. Norko, M. S. Batov, A. Otsuka, H. Yamochi, G. Saito, R. N. Lyubovskaya, *New J. Chem.* **2017**, *41*, 6866–6874.

[23] a) A. V. Zabula, S. N. Spisak, A. S. Filatov, V. M. Grigoryants, M. A. Petrukhina, *Chem. Eur. J.* **2012**, *18*, 6476–6484; b) Z. Zhou, S. N. Spisak, Q. Xu, A. Y. Rogachev, Z. Wei, M. Marcaccio, M. A. Petrukhina, *Chem. Eur. J.* **2018**, *24*, 3455–3463; c) Z. Zhou, Z. Wei, Y. Tokimaru, S. Ito, K. Nozaki, M. A. Petrukhina, *Angew. Chem. Int. Ed.* **2019**, *58*, 12107–12111; d) Z. Zhou, X. Y. Wang, Z. Wei, K. Mullen, M. A. Petrukhina, *Angew. Chem. Int. Ed.* **2019**, *58*, 14969–14973.

[24] Deposition numbers 2238944 (for **7b**) and 2238945 (for **7c**) contain the supplementary crystallographic data for this paper. These data are provided free of charge by the joint Cambridge Crystallographic Data Centre and Fachinformationszentrum Karlsruhe Access Structures service.

[25] D. Geuenich, K. Hess, F. Köhler, R. Herges, *Chem. Rev.* **2005**, *105*, 3758–3772.

[26] a) R. C. Haddon, *Acc. Chem. Res.* **1988**, *21*, 243–249; b) K. Jug, P. C. Hiberty, S. Shaik, *Chem. Rev.* **2001**, *101*, 1477–1500; c) A. Bedi, O. Gidron, *Acc. Chem. Res.* **2019**, *52*, 2482–2490; d) R. Kumar, H. Aggarwal, A. Srivastava, *Chem. Eur. J.* **2020**, *26*, 10653–10675.

[27] a) M. Stępień, E. Gońka, M. Żyła, N. Sprutta, *Chem. Rev.* **2017**, *117*, 3479–3716; b) A. Borissov, Y. K. Maurya, L. Moshniaha, W.-S. Wong, M. Żyła-Karwowska, M. Stępień, *Chem. Rev.* **2022**, *122*, 565–788.

[28] a) V. Kiran, S. P. Mathew, S. R. Cohen, I. Hernandez Delgado, J. Lacour, R. Naaman, *Adv. Mater.* **2016**, *28*, 1957–1962; b) K. Michaeli, N. Kantor-Uriel, R. Naaman, D. H. Waldeck, *Chem. Soc. Rev.* **2016**, *45*, 6478–6487; c) R. Naaman, Y. Paltiel, D. H. Waldeck, *Nat. Chem. Rev.* **2019**, *3*, 250–260.

[29] D. T. Chase, A. G. Fix, S. J. Kang, B. D. Rose, C. D. Weber, Y. Zhong, L. N. Zakharov, M. C. Lonergan, C. Nuckolls, M. M. Haley, *J. Am. Chem. Soc.* **2012**, *134*, 10349–10352.

Manuscript received: June 2, 2023
Accepted manuscript online: June 26, 2023
Version of record online: July 14, 2023

© 2023 The Authors. Angewandte Chemie International Edition published by Wiley-VCH GmbH

15213773, 2023, 34, Downloaded from https://onlinelibrary.wiley.com/doi/10.1002/anie.202307750 by MPI 355 Polymer Research, Wiley Online Library on [22/08/2023]. See the Terms and Conditions (https://onlinelibrary.wiley.com/terms-and-conditions) on Wiley Online Library for rules of use; OA articles are governed by the applicable Creative Commons License